Article



Compartmental exchange regulates steady states and stochastic switching of a phosphorylation network

Hannah N. Schmidt, Thomas K. Gaetjens, Emily E. Leopin, and Steven M. Abel, Abel, ¹Department of Chemical and Biomolecular Engineering, University of Tennessee, Knoxville, Tennessee

ABSTRACT The phosphoregulation of proteins with multiple phosphorylation sites is governed by biochemical reaction networks that can exhibit multistable behavior. However, the behavior of such networks is typically studied in a single reaction volume, while cells are spatially organized into compartments that can exchange proteins. In this work, we use stochastic simulations to study the impact of compartmentalization on a two-site phosphorylation network. We characterize steady states and fluctuation-driven transitions between them as a function of the rate of protein exchange between two compartments. Surprisingly, the average time spent in a state before stochastically switching to another depends nonmonotonically on the protein exchange rate, with the most frequent switching occurring at intermediate exchange rates. At sufficiently small exchange rates, the state of the system and mean switching time are controlled largely by fluctuations in the balance of enzymes in each compartment. This leads to negatively correlated states in the compartments. For large exchange rates, the two compartments behave as a single effective compartment. However, when the compartmental volumes are unequal, the behavior differs from a single compartment with the same total volume. These results demonstrate that exchange of proteins between distinct compartments can regulate the emergent behavior of a common signaling motif.

SIGNIFICANCE Cells are organized into compartments, as exemplified by membrane-enclosed organelles and by recent developments in the study of biomolecular condensates. However, although proteins can dynamically switch between compartments, there is no general understanding of how protein exchange impacts signaling networks. This study uses stochastic computer simulations to reveal the effect of compartmentalization on a protein phosphorylation network. It reveals the importance of the protein exchange rate in regulating emergent, steady-state properties of the network. The principles uncovered provide insight into cellular systems and may be useful when designing synthetic condensates to control biochemical reactions.

INTRODUCTION

Compartmentalization is a key organizational principle in cell biology. The interiors of cells are organized in part by membrane-enclosed organelles and their more recently discovered membraneless counterparts (1,2). However, relatively little work has explored how signaling responses are regulated by compartmentalization and the exchange of proteins between compartments.

The behavior of cell signaling networks is governed by features including topology of the reaction network, kinetic parameters, and concentrations of proteins. Spatial organization

Submitted May 18, 2023, and accepted for publication January 31, 2024.

*Correspondence: abel@utk.edu

Editor: Ramon Grima.

https://doi.org/10.1016/j.bpj.2024.01.039

© 2024 Biophysical Society.

and spatiotemporal correlations can also regulate the emergent behavior (3–7). However, spatial effects are generally less well understood, as signaling networks are most commonly studied in well-mixed settings. It is likely that compartmentalization is a regulatory mechanism for some biochemical reaction networks because it connects mesoscale organization to dynamics of signaling networks (2,8-10).

The nucleus and cytoplasm are a classic example of compartmentalization within the cell, with the regulated exchange of biomolecules between them facilitated by nuclear pore complexes (11). Other membrane-enclosed organelles exchange proteins by means of protein transporters or vesicular transport (12), and the plasma membrane and cytoplasm can be considered separate compartments when the recruitment of cytosolic proteins to the membrane is controlled by lipid or protein binding motifs (5).



Implications of compartmentalization are also interesting in light of the vast and rapidly expanding field of biomolecular condensates. Membraneless organelles are condensed, liquid-like domains that can exchange biomolecules with their surroundings (2,13,14). While much emphasis has been placed on mechanisms of their formation, relatively little is known about how they regulate biomolecular processes in cells (9,10,15,16). Phase separation of liquid phases appears to modulate membrane proximal immunecell signaling (10,17,18), and recent work has shown that, even though protein levels in cells are noisy, liquid droplets can reduce the noise in protein concentrations outside of the droplets (15,19). In addition, Sang et al. recently engineered synthetic condensates that can recruit kinase and substrate proteins (9). The synthetic condensates exhibit increased kinase activity, with the potential to broaden kinase specificity when there are multiple potential substrates. It is exciting to consider the possibility of engineering spatial control in this and other condensed systems, with the ability to partition biomolecular reaction networks between two phases. For example, macromolecular crowding was used to differentially organize components of cell-free protein synthesis. impacting the output of gene expression (20,21).

The phosphoregulation of proteins is an important regulatory mechanism in cells. Kinases and phosphatases regulate the phosphorylation and dephosphorylation, respectively, of many proteins. Mitogen-activated protein kinase (MAPK) cascades are some of the most-studied signaling pathways in eukaryotic cells, propagating signals from the plasma membrane to the nucleus, enabling dynamic signal processing, and regulating many downstream processes (9,22-25). Other well-studied examples include networks involved in control of the cell cycle and in the phosphorylation of the cytoplasmic tail of the T cell receptor complex (26).

In MAPK cascades, multisite phosphorylation provides a mechanism to control protein activity, leading to emergent behavior including ultrasensitivity and bistability (24,27– 30). Even a single leaflet of the MAPK cascade can exhibit bistability when kinases and phosphatases bind in a distributive manner (i.e., they unbind after each enzymatic modification) (31). Bistability describes the ability of a network to exist in one of two stable steady states; it is a common feature of signaling networks that allows cells to make binary decisions (32). More generally, networks can exhibit multistability, in which there are two or more stable steady states. Interestingly, Harrington et al. showed that exchange of select species between two compartments can lead to bistability in an otherwise monostable reaction network. They focused on the regulation of a substrate protein with a single phosphorylation site, demonstrating that compartmentalization expands the emergent behavior possible (25).

In multistable systems, fluctuations associated with stochastic reaction kinetics can lead to stochastic switching between steady states (33–35). Behavior in such systems is typically characterized by long residence times in steady

states, interspersed by rapid transitions between them (36,37). Spatial effects can shape the likelihood of stochastic switching in bistable networks (38,39), but little is known about the impact of compartmentalization when components can exchange between compartments.

This paper explores the impact of compartmentalization on a network in which the phosphorylation states of substrate proteins are regulated by kinases and phosphatases. We were first inspired, on a conceptual level, by the work of Sang et al., who engineered synthetic condensates that could recruit kinases and substrate proteins (9). However, we are interested in compartmentalization in general, so we have chosen a common phosphoregulation motif and a general model of the compartments. We systematically vary the exchange rate between the compartments to account for a variety of possible biological compartments and exchange mechanisms.

The signaling network is motivated by a single leaflet of the MAPK network. It also provides insight into other networks involving the phosphoregulation of substrate proteins with multiple phosphorylation sites, as described in previous studies (3,4). We use stochastic, particle-based simulations to characterize steady states and stochastic switching between them. We first characterize behavior in a single, well-mixed compartment before systematically varying the exchange rate of particles between two compartments, each of which is well mixed. We then study the effects of particle exchange between compartments of different volumes. Taken together, our work emphasizes that compartmentalization and protein exchange can regulate the emergent behavior of common signaling motifs.

METHODS

We use the Gillespie algorithm (40) to simulate the time evolution of a distributive, two-site phosphorylation network in two coupled compartments. The system is assumed to be well-mixed in each compartment, and proteins exchange between compartments with rate k_{EX} . The network contains substrate proteins that can be phosphorylated at two sites: a kinase (E) catalyzes the phosphorylation of an unphosphorylated residue and a phosphatase (P) catalyzes the dephosphorylation of a phosphorylated residue. Each substrate protein can have no sites (S_0) , one site (S_1) , or both sites (S2) phosphorylated. In distributive reaction networks, enzymes unbind from the substrate they are modifying after each catalytic step (31,41). The following reactions specify the network in compartment i (= A or B):

$$S_{0,i}+E_i \xrightarrow[k_2]{k_1} S_{0,i}E_i \xrightarrow{k_3} S_{1,i}+E_i$$

$$S_{1,i}+E_i \stackrel{\underline{k_4}}{\rightleftharpoons} S_{1,i}E_i \stackrel{k_6}{\rightarrow} S_{2,i}+E_i$$

$$S_{2,i} + P_i \xrightarrow[k_2]{k_1} S_{2,i} P_i \xrightarrow{k_3} S_{1,i} + P_i$$

$$S_{1,i} + P_i \xrightarrow[\overline{k_6}]{k_4} S_{1,i} P_i \xrightarrow{k_6} S_{0,i} + P_i$$

The compartments are coupled by the exchange of particles: each protein or protein complex in compartment A transitions to compartment B with rate k_{EX} , and vice versa. We use the kinetic parameters in Table 1, which are based on previous studies (3,4). The exchange rate is systematically varied from 10^{-3} to 1 s^{-1} to characterize the impact on steady states and the transitions between them. This range is consistent with nuclear import and export rates for the MAPK proteins Erk1 and Erk2, which have been estimated to range from 1.4×10^{-3} to 5.4×10^{-1} s⁻¹ depending on cell type and context (42). Exchange rates for biomolecular condensates can also vary over a wide range (43).

The system is initialized with 50 S_0 , 50 S_2 , 25 E, and 25 P in each compartment. The volume of the compartments is varied to characterize the effect of particle concentration. In the Gillespie simulations, which are formulated in terms of particle numbers, second order rates (k_1 and k_4) are divided by the compartmental volume to account for concentration effects. We assume that the exchange of particles between compartments is a first-order process that is independent of the volume of the system. Thus, when the compartmental volumes are unequal, each compartment has the same average number of particles but a different concentration. For diffusion coefficients associated with diffusion in the cytoplasm, at the plasma membrane, and in some biomolecular condensates (44), the characteristic time to diffuse across domains of the size considered here is less than the shortest characteristic time for a particle to exchange between compartments. Thus, we assume that the compartments are well mixed and that exchange rates are not diffusion influenced.

Because of the symmetry between kinase and phosphatase reactions, the initial conditions chosen provide an unbiased initial state. For each condition studied, we generate 1000 independent trajectories, each of which is 10,000 s in duration. The state of the system is recorded every 0.1 s, and the first 100 s of each trajectory are excluded from calculations to allow the system to reach steady state. We characterize the correlation coefficient between two random variables X and Y as $\rho_{XY} = \langle (X - \langle X \rangle)(Y - \langle Y \rangle) \rangle / \langle Y \rangle$ $\sigma_X \sigma_Y$, where angular brackets represent an average and σ_i denotes the standard deviation.

We also consider the deterministic, mean-field behavior of the system and numerically solve the system of ordinary differential equations (ODEs) describing the mass-action kinetics of the reaction network. We sample initial conditions throughout state space and use ode45 in MATLAB to numerically integrate the ODEs until steady state is achieved. Using this approach, we identify stable, steady-state solutions as a function of the volume of the compartments and the exchange rate between them.

TABLE 1 Kinetic parameters for the reaction network

Kinetic parameter	Value	Related reactions
k_1	$0.045 \ \mu \text{m}^3 \ \text{s}^{-1}$	$S_0 + E \rightarrow S_0 E$
		$S_2 + P \rightarrow S_2 P$
k_2	1.35 s^{-1}	$S_0E \rightarrow S_0 + E$
	1	$S_2P \rightarrow S_2 + P$
k_3	1.5 s^{-1}	$S_0E \rightarrow S_1 + E$
	0.000 3 -1	$S_2P \rightarrow S_1 + P$
k_4	$0.093 \ \mu \text{m}^3 \text{ s}^{-1}$	$S_1 + E \rightarrow S_1 E$
1	1.73 s^{-1}	$S_1 + P \rightarrow S_1 P$
k_5	1./3 S	$S_1E \rightarrow S_1 + E$
t.	$15 \mathrm{s}^{-1}$	$S_1P \rightarrow S_1 + P$ $S_1E \rightarrow S_2 + E$
k_6	13 8	$S_1E \rightarrow S_2 + E$ $S_1P \rightarrow S_0 + P$
k_{EX}	varied (s ⁻¹)	$E_A \leftrightarrow E_R$
	,	$P_A \leftrightarrow P_B$
		$S_{x,A} \leftrightarrow S_{x,B}$
		$S_{x,A}E_A \leftrightarrow S_{x,B}E_B$
		$S_{x,A}P_A \leftrightarrow S_{x,B}P_B$

Reactions associated with rates k_1 to k_6 take place in compartments A and B (subscripts are omitted for clarity).

Detecting stochastic switches

When in a multistable regime, the system can stochastically switch between steady states due to intrinsic fluctuations in the system. To identify stochastic switches, we use a heuristic algorithm that analyzes time traces of the number of S_2 molecules (N_{S_2}) in each compartment. We identify switches by assessing when the moving average of N_{S_2} crosses a threshold value approximately equal to the value of the unstable steady state identified from analysis of the deterministic equations near the critical point $(N_{S_2} = 35)$. Specifically, we calculate a moving average with a time window of 10 s and classify a switching event in a compartment when the moving average crosses the threshold for at least 1 s. This reduces the overclassification of short-lived fluctuations as switching events. We use this information to determine the distribution of residence times in each steady state and to quantify the mean switching time, τ , which is the average residence time in a state before stochastically switching to another. For an exponentially distributed random variable, τ^{-1} gives the rate parameter of the distribution.

DATA AND CODE AVAILABILITY

Simulation and analysis code used in this work is available at https://github.com/schmidthn17/Schmidt2023Exchange.

RESULTS AND DISCUSSION

An isolated compartment exhibits bistability at sufficiently high concentrations

We begin by analyzing the reaction network in a single, wellmixed compartment. We fix the number of proteins (100 substrate proteins, 25 kinases, and 25 phosphatases) and vary the volume. Fig. 1 shows the number of fully phosphorylated substrate particles (N_{S_2}) at steady state, as determined by stochastic simulations (red points) and numerical solutions of the ODEs associated with deterministic, mass-action kinetics (black lines). The deterministic solutions highlight a pitchfork bifurcation, with the system bistable at sufficiently small volumes and monostable at larger volumes. Below a critical volume ($\approx 0.46 \,\mu\text{m}^3$), there are two stable steady states (solid lines) and one unstable steady state (dashed line) between them. Above the critical volume, there is a single stable steady state. For the stochastic simulations, we characterize the distribution of the number of S_2 molecules. At sufficiently small volumes, the distribution is bimodal, and the location of each mode (red dot) is close to a stable deterministic solution. The distribution consists of a single mode in the monostable regime. The mean switching times in the bistable regime are characterized in Fig. S1.

In the bistable region, we refer to the state with more S_2 particles as the *active state* and the state with fewer S_2 particles as the *inactive state*. The behavior in Fig. 1 is a consequence of changing concentration: The number of particles in the system is constant, so a smaller volume results in a larger concentration. For the two-site distributive reaction network, bistability arises from a sequestration effect when the number of substrate proteins exceeds the number of enzymes (4,31). When the system is in the active state

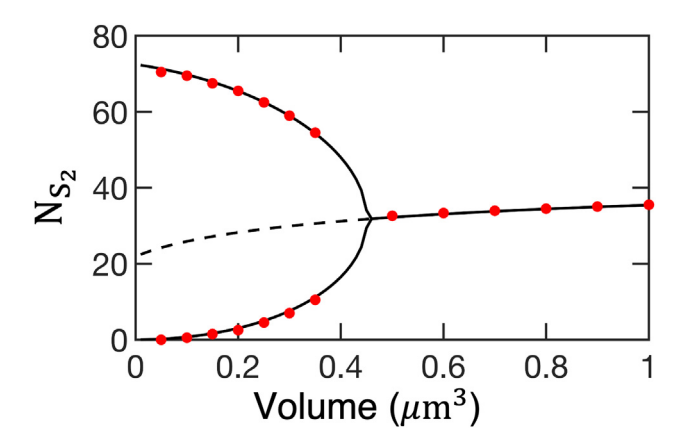


FIGURE 1 Number of S_2 particles at steady state in a single, well-mixed volume, as determined by deterministic (black lines) and stochastic (red circles) methods. Solid lines denote stable steady states and the dashed line denotes an unstable steady state. Results from stochastic simulations correspond to the mode(s) of the distribution of N_{S_2} . Mean switching times between states in the bistable regime, obtained from stochastic simulations, can be found in Fig. S1. To see this figure in color, go online.

 $(N_{S_2} > N_{S_0})$, more phosphatases are typically bound than kinases. When a protein is dephosphorylated, the phosphatase unbinds, and there are more kinases than phosphatases available to bind to the now singly-phosphorylated protein. Thus, it is more likely to return to the fully phosphorylated state. An analogous argument holds for the inactive state $(N_{S_0} > N_{S_2})$, where the kinases are sequestered and there is an excess of phosphatases available to bind. Larger concentrations promote protein binding, which enhances the sequestration effect needed for bistability.

The exchange rate controls steady states and correlation between compartments

For the remainder of the paper, we consider a system with two compartments (A and B). Each compartment is assumed to be well mixed, and particles exchange between the compartments with rate k_{EX} . Initially, we consider compartments of equal volume, with $V_A = V_B = 0.16$, 0.24, 0.32, and $0.4 \,\mu\text{m}^3$. These volumes are within the bistable region identified in Fig. 1 for a single compartment. Focusing on equal volumes allows us to examine the impact of particle exchange without confounding effects of different volumes. We later explore the effect of pairing compartments with $V_A \neq V_B$ when, in the absence of exchange, compartment A would be bistable and compartment *B* would be monostable. When $k_{EX} = 0$, there is no particle exchange, and the compartments evolve independently. In this limit, each compartment is equivalent to a case considered in an isolated compartment exhibits bistability at sufficiently high concentrations.

We first characterize stable steady states of the deterministic, mean-field system of ODEs describing the reaction network in two compartments. Figs. 2, A and B show the number of S_2 particles in each compartment as the exchange rate is varied. For $V_A = V_B = 0.32 \,\mu\text{m}^3$, there are four stable steady states at low values of k_{EX} . Two of the steady states are characterized by $N_{S_{2,A}} = N_{S_{2,B}}$. In these states, both compartments are either in an active regime or an inactive regime. The other two steady states are characterized by $N_{S_{2,A}} \neq N_{S_{2,B}}$. In these states, one compartment is in an active regime while the other is in an inactive regime. As the exchange rate increases, there is a transition in the number of stable steady states, and only the two states with $N_{S_{2,A}}=N_{S_{2,B}}$ persist (Fig. 2 C). For compartments with mixed volumes ($V_A = 0.32 \, \mu \text{m}^3$, $V_B = 0.8 \, \mu \text{m}^3$), there are two stable steady states at low exchange rates that transition to a single stable state as the exchange rate increases (Fig. 2D).

Fig. 3 shows results from stochastic simulations with $V_A = V_B = 0.32 \,\mu\text{m}^3$. The upper panel shows the time dependence of N_S , in compartments A and B for a portion of a single simulation trajectory for three different exchange rates. For each exchange rate, each compartment exhibits two distinct states with stochastic switching between them. At $k_{EX} = 0 \text{ s}^{-1}$, the compartments behave independently of each other. When $k_{EX} = 0.01 \text{ s}^{-1}$, the switching events in the two compartments appear to occur at similar times, and the states of compartments A and B appear to be negatively correlated: When compartment A is in an active state, compartment B tends to be in an inactive state, and vice versa. When $k_{EX} = 1 \text{ s}^{-1}$, the states of the two compartments are highly correlated, with both compartments having similar time dependence.

The lower panel in Fig. 3 shows the simultaneous distribution of the number of S_2 particles in compartments Aand B. With $k_{EX} = 0 \text{ s}^{-1}$, the compartments evolve independently, and each undergoes independent stochastic switches between steady states. This is reflected in the four regions of high frequency in the two-dimensional distribution: the four states are associated with each compartment being either active or inactive, independent of the other. In contrast, the distribution for $k_{EX} = 0.01 \text{ s}^{-1} \text{ dem}$ onstrates the negative correlation suggested by the sample trajectory. The vast majority of the weight is associated with compartment A being active while compartment B is inactive, and vice versa. The active state is shifted to larger numbers of S_2 molecules compared with $k_{EX} = 0 \text{ s}^{-1}$, and the shape of the distribution around the steady state also changes, with a larger range of N_{S_2} sampled. Although the stochastic results are in qualitative agreement with the deterministic steady states for this exchange rate (Fig. 2), the deterministic results do not reveal the relative weight of the negatively correlated states. Furthermore, they are not in quantitative agreement, with the stochastic simulations sampling larger values of N_{S_2} in the active state. At the highest exchange rate, $k_{EX} = 1 \text{ s}^{-1}$, the distribution reflects the highly correlated time traces, with most of the weight associated with states in which both compartments are either

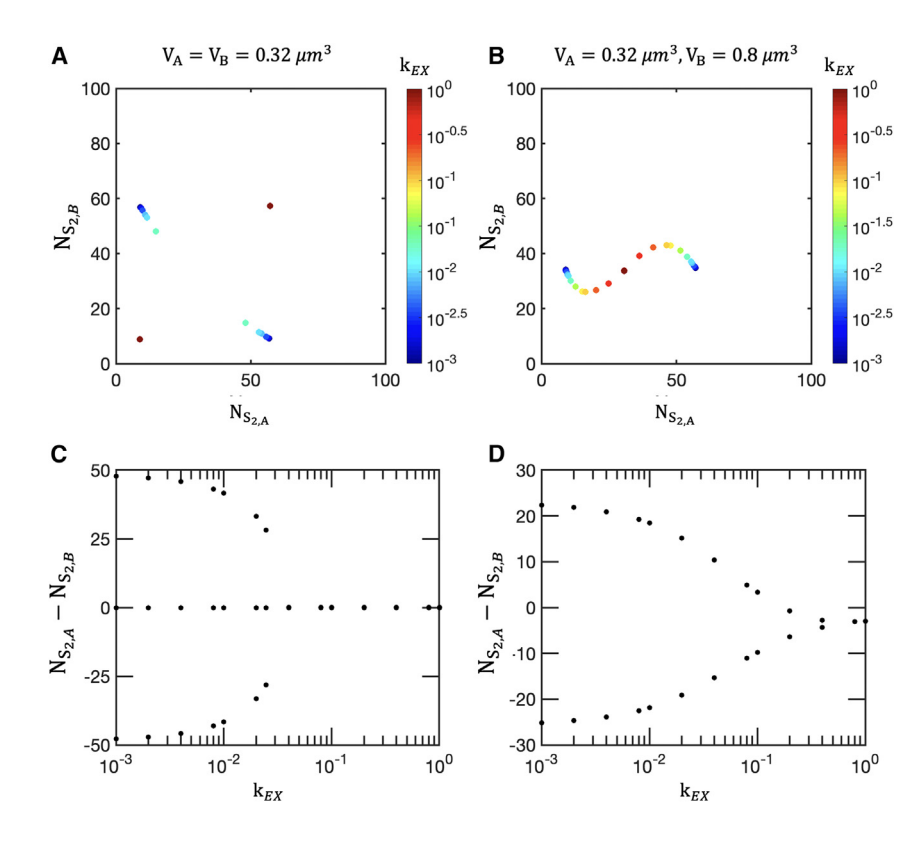


FIGURE 2 Stable steady states of the deterministic, two-compartment system. Top row: each point represents the number of S2 particles in compartments A and B at steady state. Points are color coded by the exchange rate. (A) $V_A = V_B = 0.32 \ \mu \text{m}^3$. The two states with $N_{S_{2,A}} = N_{S_{2,B}}$ are stable for every exchange rate, so the points are overlapping and appear as a single point. (B) $V_A = 0.32 \ \mu \text{m}^3$ and $V_B = 0.8 \ \mu \text{m}^3$. Bottom row: difference in the number of S_2 particles in compartments A and B as a function of the exchange rate. $V_A = V_B = 0.32 \,\mu\text{m}^3$. Note that two steady states give rise to $N_{S_{2,A}} - N_{S_{2,B}} = 0$. (D) $V_A = 0.32$ μm^3 and $V_B = 0.8 \ \mu \text{m}^3$. To see this figure in color,

active or inactive. Distributions obtained with other exchange rates are shown in Fig. S2 and illustrate the transition between the negatively and positively correlated distributions. Fig. S3 shows the distribution of N_{S_2} in a single compartment for various exchange rates, allowing direct comparison of the results in a single compartment.

To further characterize correlations between the states of the compartments, Fig. 4 A shows the correlation coefficient

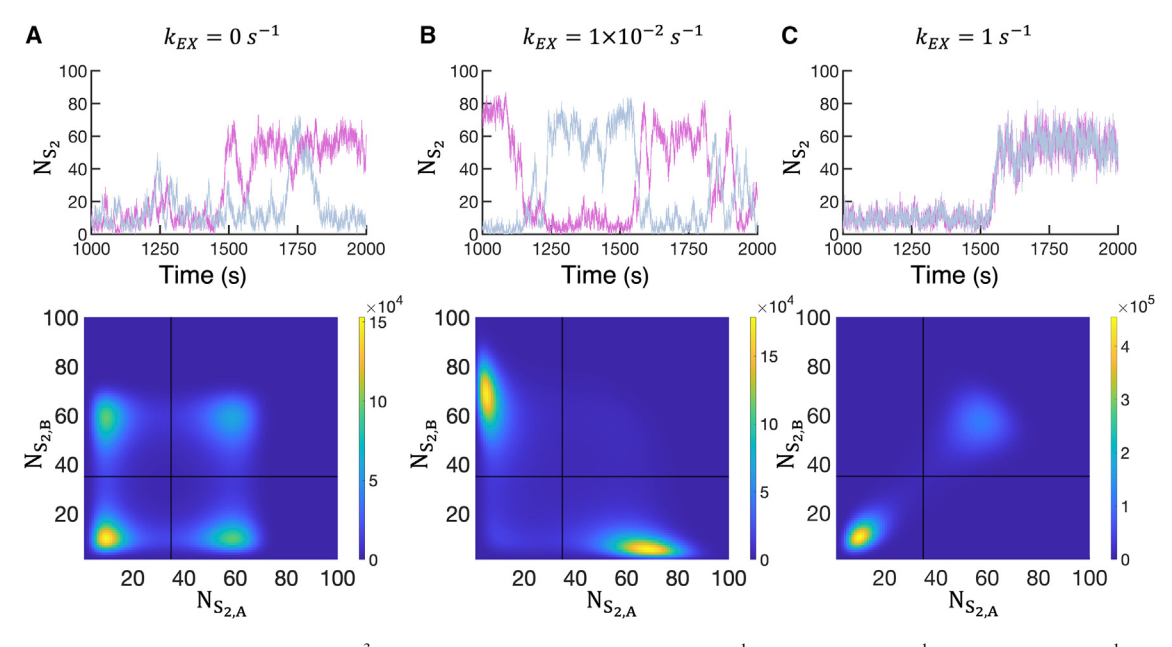


FIGURE 3 Behavior with $V_A = V_B = 0.32 \ \mu\text{m}^3$ at various exchange rates: (A) $k_{EX} = 0 \ \text{s}^{-1}$, (B) $k_{EX} = 0.01 \ \text{s}^{-1}$, and (C) $k_{EX} = 1 \ \text{s}^{-1}$. The top panel shows the number of S₂ particles in compartment A (fuchsia) and compartment B (blue) from part of a single trajectory. The bottom panel shows the distribution of S₂ particles in compartments A and B sampled from 1000 independent trajectories. Horizontal and vertical black lines denote the threshold $(N_{S_2} = 35)$ used to identify switches. To see this figure in color, go online.

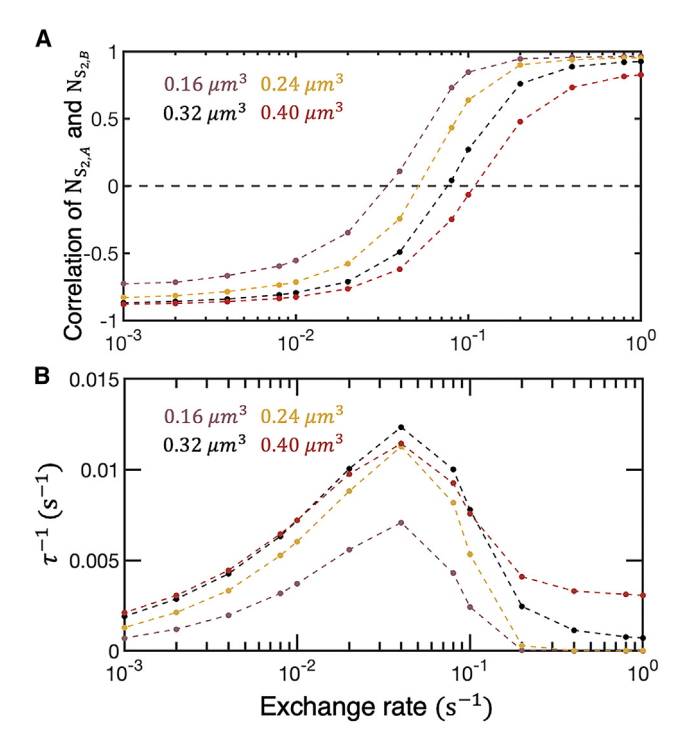


FIGURE 4 (A) Correlation between compartments as characterized by the correlation coefficient between $N_{S_{2A}}$ and $N_{S_{2B}}$. The dashed line is the correlation obtained for $k_{EX}=0~{\rm s}^{-1}$ and $V_A=V_B=0.32~\mu{\rm m}^3$. As the exchange rate increases, the compartments transition from negatively to positively correlated. (B) The inverse mean switching time (τ^{-1}) as a function of exchange rate. Each data point is obtained from 1000 trajectories. Results for $k_{EX} = 0 \text{ s}^{-1}$ are shown in Fig. S1. To see this figure in color, go online.

between $N_{S_{2,A}}$ and $N_{S_{2,B}}$. Each volume exhibits a similar shape: At low exchange rates, the correlation coefficient is < 0, indicating that the states of the two compartments are negatively correlated. At the lowest exchange rates considered, the correlation coefficient appears to approach a plateau associated with a highly anticorrelated state. As the exchange rate increases, the system switches from negatively to positively correlated. At high exchange rates, the correlation coefficient approaches 1, and the compartments are almost always in the same state (Fig. S4). As the volume increases, the transition from negative to positive correlation between the compartments occurs at higher exchange rates.

Stochastic switching is promoted at intermediate exchange rates

The sample trajectories shown in Fig. 3 suggest a change in the frequency of stochastic switching as the exchange rate is varied. In Fig. 4 B, we show the inverse mean switching time (τ^{-1}) as a function of the exchange rate for different volumes. Note that the mean switching time is defined in terms of switching for a single compartment. This facilitates comparison to the single-compartment case and to cases with compartments of different volumes. Symmetry between kinase and phosphatase reactions implies that the distribution of switching times from inactive to active states is the same as that from active to inactive. We confirm this by comparing the cumulative distribution functions obtained from simulation results, which are virtually indistinguishable (Fig. S5). We further use quantile-quantile plots to compare the switching times from simulations to an exponential distribution (Fig. S5). The switching times are exponentially distributed for isolated compartments and for sufficiently large exchange rates ($k_{EX} = 0$ and 0.04 s⁻¹). However, for small values of the exchange rate $(k_{EX} = 0.001 \text{ s}^{-1})$, the distribution deviates modestly from an exponential distribution. Thus, for isolated compartments or a large exchange rate, the inverse mean switching time can be regarded as the rate parameter of an exponential distribution.

Fig. 4 B reveals that the inverse mean switching time is a nonmonotonic function of the exchange rate, and that the maximum occurs at intermediate exchange rates. At low exchange rates, τ^{-1} increases with increasing exchange rate. It then peaks at intermediate exchange rates, before rapidly falling to a plateau at higher exchange rates. Smaller volumes exhibit less frequent stochastic switching. However, the differences are modest at low and intermediate exchange rates when compared with isolated compartments. With $k_{EX} = 10^{-3} \text{ s}^{-1}$, the largest volume switches ≈ 3 times more frequently than the smallest volume. In contrast, when $k_{EX} = 0 \text{ s}^{-1}$, the largest volume switches ≈ 8600 times more frequently than the smallest volume (Fig. S1).

For large exchange rates, the differences in the mean switching times between different volumes are more pronounced. In this regime, no switching events were observed for $V_A = V_B = 0.16 \ \mu\text{m}^3$, whereas $\tau^{-1} \approx 0.003 \ \text{s}^{-1}$ for $V_A = V_B = 0.40 \ \mu\text{m}^3$ (Fig. S1). Physically, the two compartments behave like a well-mixed system with a larger effective volume $(V = V_A + V_B)$. To test this, we consider a single compartment with total volume V and the same total number of particles. Fig. S6 shows that, when the exchange rate is large, the distribution of the total number of S_2 particles in both compartments is almost indistinguishable from the distribution of the larger single compartment. Because of the larger number of particles at the same concentration, the impact of intrinsic fluctuations is reduced, thus suppressing stochastic switching when the exchange rate is large (Fig. S1) (33,45).

Fluctuations in the balance of enzymes influence steady states at low and intermediate exchange rates

Fig. 4 B shows that the rate of particle exchange influences the mean switching time. Furthermore, Figs. 3 and S2 reveal, at low and intermediate exchange rates, a negative correlation between the compartments, an increase in the value of N_{S_2} in the active state, and a broadening of the distribution associated with the active state. Taken together, these results suggest a mechanism for stochastic switching that is influenced by the balance of enzymes in the compartments and the timescale of their fluctuations.

To test this, we characterize Δ_{EP} , the difference in the total number of kinases and phosphatases in a compartment (the total includes both free and bound enzymes). Fig. 5, A and B show sample trajectories in which the time dependence of Δ_{EP} is plotted with N_{S_2} in the same compartment. With $k_{EX} = 0.01 \text{ s}^{-1}$, there is a strong correlation between fluctuations of Δ_{EP} and N_S ,: when $\Delta_{EP} > 0$, the compartment is likely to be in an active state, and when $\Delta_{EP} < 0$, the compartment is likely to be in an inactive state. In contrast, with $k_{EX} = 1 \text{ s}^{-1}$, the fluctuations of Δ_{EP} occur on shorter timescales and appear uncorrelated with the state of the compartment.

To further explore the relationship between Δ_{EP} and the state of the compartment, we calculate the correlation coefficient between Δ_{EP} and $N_{S_{2,A}}$. Fig. 5 C shows that Δ_{EP} is strongly correlated with $N_{S_{2,A}}$, and hence the state of the compartment, at low exchange rates. The correlation decreases with increasing exchange rate and becomes uncorrelated at higher exchange rates. Thus, at low and intermediate exchange rates, when there are more phosphatases than kinases in a compartment, the compartment tends to be in the inactive state; similarly, when there are more kinases than phosphatases, the compartment tends to be in the active state. Changes in the balance of enzymes influence the transitions between active and inactive states. Other dynamical variables considered do not show strong correlation with the state of the system. For example, it is plausible that fluctuations in the total number of substrate particles in a compartment could bias the state of the network due to sequestration effects. We examine the correlation coefficient between $N_{S_{2,4}}$ and the total number of substrate particles in compartment A (Fig. S7), which shows only weak correlation across all exchange rates.

In Fig. 6, we further characterize the relation between the balance of enzymes and the state of the compartment. Here, we show the conditional distribution of N_{S_2} in a compartment given a specific value of Δ_{EP} . For $k_{EX} = 0$ s⁻¹, there is no enzyme exchange and $\Delta_{EP} = 0$ for the entire simulation. This case gives the steady-state distribution of N_{S_2} in the absence of exchange. With $k_{EX} = 0.01 \text{ s}^{-1}$, the distribution with $\Delta_{EP} = 0$ is similar to the case with no exchange, with the distribution slightly broadened about each mode. As Δ_{EP} increases, indicating more kinases than phosphatases, the weight associated with the active state increases and the mode shifts to larger values. With $\Delta_{EP} = 8$, there is only a single mode, indicating that the imbalance in enzymes biases the system to a single active state. Similarly, with $\Delta_{FP} < 0$, the excess of phosphatases biases the system to an inactive state. In this regime, as Δ_{EP} decreases, the weight associated with the inactive state increases and the mode shifts to smaller values. In contrast, with fast exchange between compartments

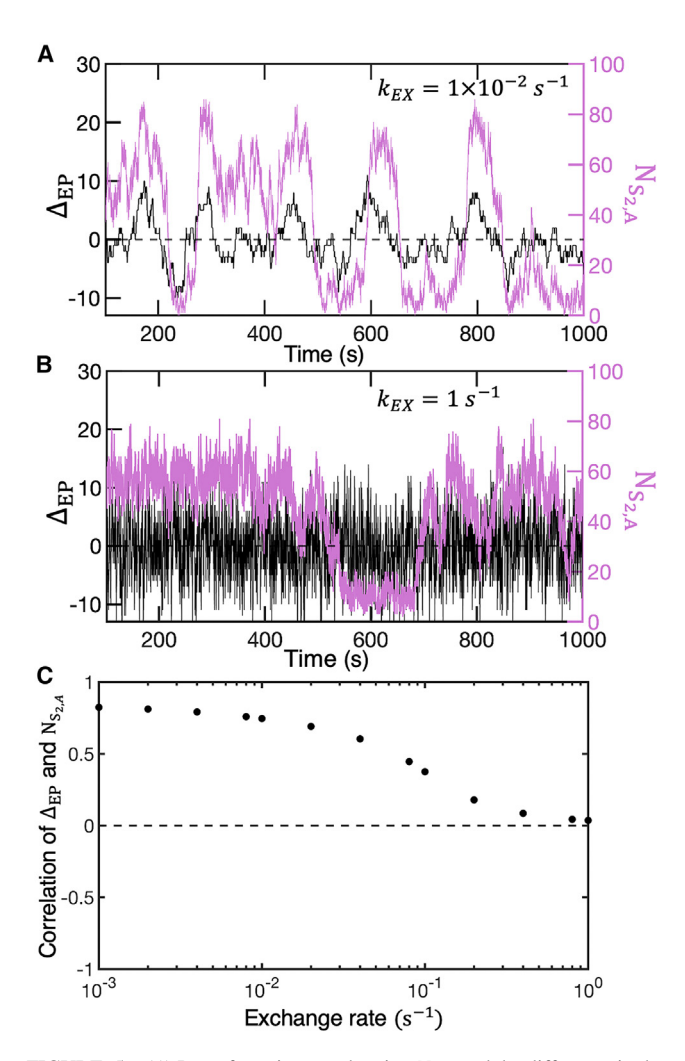


FIGURE 5 (A) Part of a trajectory showing $N_{S_{2,4}}$ and the difference in the number of kinases and phosphatases (Δ_{EP}) in compartment A as a function of time for $k_{EX}=1\times 10^{-2}\,\mathrm{s}^{-1}$ and $V_A=V_B=0.32\,\mu\mathrm{m}^3$. (B) Analogous results with $k_{EX} = 1 \text{ s}^{-1}$. (C) Correlation coefficient between Δ_{EP} and $N_{S_{2,A}}$ (1000 trajectories for each exchange rate). As the exchange rate between compartments increases, the state of the system (represented by $N_{S_{2,4}}$) and Δ_{EP} become uncorrelated. To see this figure in color, go online.

 $(k_{EX} = 1 \text{ s}^{-1})$, the distributions show almost no dependence on Δ_{EP} in the range considered. This is consistent with the results of Fig. 5 showing no correlation between enzyme fluctuations and the state of the system.

The bias introduced by imbalances in the enzymes leads to the negative correlation between the state of each compartment at low and intermediate exchange rates (Fig. 4 A). Because of particle conservation, an excess of kinases in compartment A implies an excess of phosphatases in compartment B, thus leading to anticorrelated states. The negative correlation is expected to persist for lower exchange rates. In this regime, as the exchange rate becomes arbitrarily small, the time between exchange events becomes arbitrarily long. Thus, between exchange events, each compartment is effectively isolated and at a steady state associated with a particular allocation of particles between

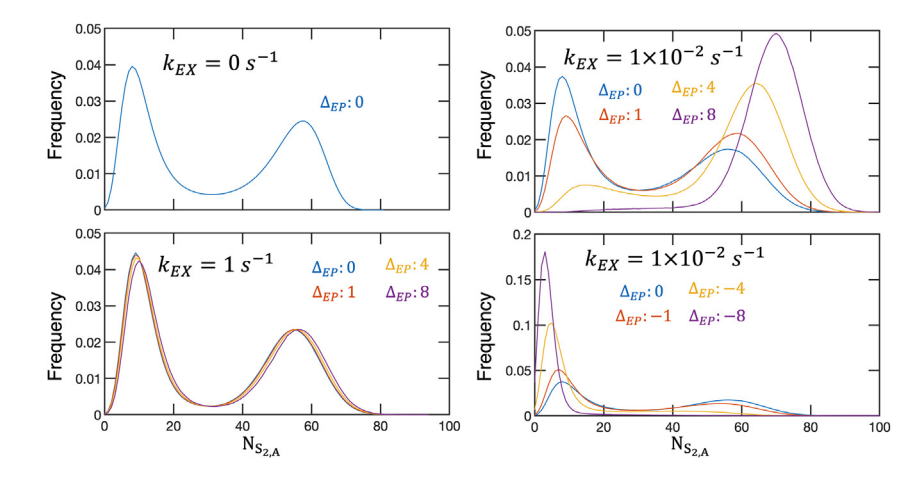


FIGURE 6 Conditional distribution of N_{S_2} given specific values of Δ_{EP} . Three exchange rates are shown with $V_A = V_B = 0.32 \ \mu \text{m}^3$. Results are obtained from 1000 independent trajectories. To see this figure in color, go online.

the compartments. Rare particle exchange events would then lead to each compartment residing in a new effective steady state. To properly sample the full distribution of possible states, the simulation time would need to be sufficiently long to sample the full distribution of particle allocations. The negative correlation will thus plateau at a level consistent with an ensemble of effective steady states associated with rare changes in the allocation of particles. Note that $k_{EX} = 0$ s⁻¹ exhibits qualitatively different behavior because the distribution of enzymes and substrate particles between compartments never changes. With no exchange, the correlation coefficient between $N_{S_{2,A}}$ and $N_{S_{2,B}}$ is zero.

Fluctuations in the balance of enzymes are a primary mechanism driving transitions between states at lower exchange rates. However, there is no obvious dynamical variable or reaction coordinate that provides a mechanistic understanding of transitions between states at higher exchange rates. Stochastic switching events arise because spontaneous fluctuations reverse the sequestration effect, but the reaction pathways responsible for this are uncharacterized even in a single reaction volume. Characterizing such transitions using transition path theory to identify transition bottlenecks (46) would be an interesting future direction, both in isolated and compartmentalized systems.

Coupling compartments of different sizes

Our results thus far have emphasized the importance of particle exchange between compartments when the average concentration is equal in each. In biological systems, it is common to encounter compartments with different effective concentrations of proteins. In this section, we consider two compartments with the same numbers of particles as above but with different volumes: $V_A = 0.32 \ \mu \text{m}^3$ and $V_B = 0.8$ or $10 \ \mu \text{m}^3$. With no exchange, compartment A is in the bistable regime and compartment B is in the monostable regime (Fig. 1).

Fig. 7 shows, for $V_A = 0.32 \ \mu\text{m}^3$ and $V_B = 0.8 \ \mu\text{m}^3$, sample trajectories (*upper panel*) and the distribution of

the number of S_2 particles in compartments A and B (lower panel) for three exchange rates. With $k_{EX} = 0 \text{ s}^{-1}$, the results reflect the bistable behavior in compartment A and monostable behavior in compartment B. With $k_{EX} = 0.01$ s⁻¹, there remain two steady states, as can be seen in the distribution. However, compared to the case of no exchange, they are shifted, broadened, and negatively correlated. In compartment A, the active state is shifted to larger values of $N_{S_2,A}$ and the inactive state is shifted to smaller values. In addition, the distribution around each steady state exhibits negative correlation between $N_{S_2,A}$ and $N_{S_2,B}$. This behavior is conceptually similar to that with $V_A = V_B$, suggesting that the balance of kinases and phosphatases is again important in controlling the state of the system. With fast exchange ($k_{EX} = 1 \text{ s}^{-1}$), the system is monostable, as indicated by the single peak in the distribution. The states of compartments A and B are highly correlated, as seen in the trajectory and in the strong positive correlation in the distribution. The fluctuations are large, leading to a broad distribution of N_{S_2} in each compartment. Distributions for additional exchange rates are shown in Fig. S8 A.

The behavior of the system with $V_A = 0.32 \ \mu \text{m}^3$ and $V_B = 10 \ \mu \text{m}^3$ is similar (Fig. S8 B), except that at low and intermediate exchange rates, the distribution of $N_{S_{2B}}$ is narrower. In this regime of exchange rates, enzyme imbalances remain important. However, because of the large volume of compartment B, enzymes are less likely to bind to substrates, thus reducing the effect of fluctuations in the balance of kinases and phosphatases in the larger compartment.

We further characterize the inverse mean switching time (τ^{-1}) in compartment A for exchange rates at which it exhibits bistable behavior. These results are shown in Fig. 8 for $V_A = 0.32~\mu\text{m}^3$ and $V_B = 0.32$, 0.8, and 10 μm^3 . In the slow-exchange regime, the behavior of the three cases is essentially indistinguishable. At intermediate exchange rates, coupling to larger compartments causes the peak of τ^{-1} to shift to modestly higher exchange rates, but the shape of the response is qualitatively similar. The inverse mean switching time starts to decrease after the peak, but the

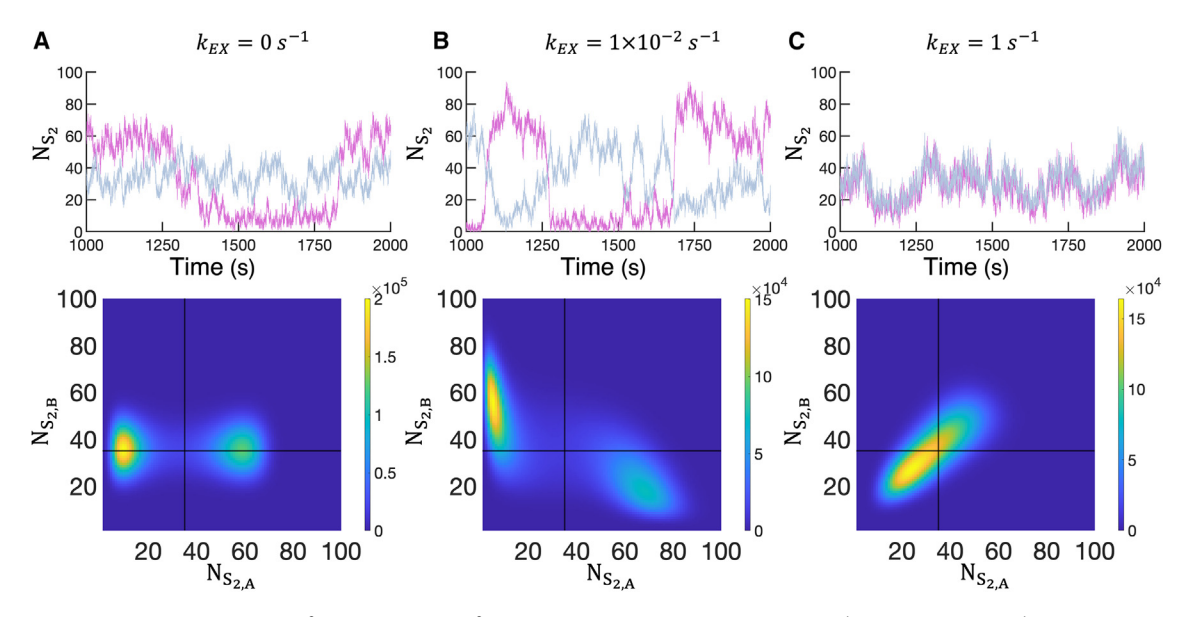


FIGURE 7 Behavior with $V_A = 0.32 \, \mu\text{m}^3$ and $V_B = 0.8 \, \mu\text{m}^3$ at various exchange rates: (A) $k_{EX} = 0 \, \text{s}^{-1}$, (B) $k_{EX} = 0.01 \, \text{s}^{-1}$, and (C) $k_{EX} = 1 \, \text{s}^{-1}$. The top panel shows the number of S_2 particles in compartment A (fuchsia) and compartment B (blue) from part of a single trajectory. The bottom panel shows the distribution of S_2 particles in compartments A and B sampled from 1000 independent trajectories. To see this figure in color, go online.

system becomes monostable. These results indicate that the switching behavior of a compartment at low exchange rates is largely dependent on fluctuations in particle numbers due to exchange between the compartments, and not directly on the state of the other compartment.

For large exchange rates, the states of two compartments are highly correlated. Particles rapidly switch between compartments and thus effectively sample volume $V = V_A + V_B$ over short timescales. To this end, we compare the results with two compartments at large exchange rates (k_{EX} = 1, 10, and $100 \,\mathrm{s}^{-1}$) with the equivalent single-compartment system of volume V (containing the same total number of each protein). Figs. 9, A and B compare the distribution of the total number S_2 particles in two compartments with the number of S_2 particles in the equivalent single compartment. The distributions are unimodal but markedly different in shape. With two compartments, the distribution is broader, indicating that the interplay between the two compartments is more complex than simply combining the two volumes. These results are in contrast with Fig. S6, which shows that fast exchange with $V_A = V_B$ leads to a steady state that is nearly indistinguishable from the equivalent single compartment.

CONCLUSION

Compartmentalization is a cornerstone of cell biology. Membrane-enclosed organelles such as the nucleus exchange proteins with the cytoplasm, with translocation of MAP kinases being one prominent example (7,11). Proteins can be recruited from the cytoplasm to the plasma membrane, creating two effective compartments (8,47), and liquid-liquid phase separation leads to distinct, membraneless domains that can be found in the cytoplasm, the nucleus, and the plasma membrane (1,14,48). In all cases, proteins can dynamically exchange between different compartments and thus potentially impact signal transduction and other cellular processes. Various biophysical mechanisms can facilitate protein exchange, with rates of exchange varying over orders of magnitude.

Relatively little is known about the effects of compartmentalization and the exchange of proteins on the emergent behavior of signaling networks. To gain insight, we studied a common signaling motif describing the phosphoregulation of substrate proteins by kinases and phosphatases. The network and parameters were motivated by a leaflet of the MAPK pathway, which can exhibit bistability due to the sequestration of enzymes at sufficiently high concentrations. Our key results are highlighted in Fig. 4, which reveals that

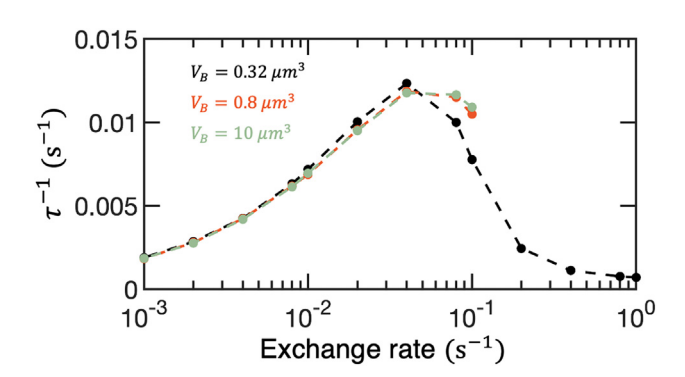


FIGURE 8 The inverse mean switching time (τ^{-1}) in compartment A as a function of exchange rate when $V_A = 0.32 \ \mu \text{m}^3$ and $V_B = 0.32, 0.8, \text{ or}$ 10 μ m³. Results with $V_B = 0.32 \ \mu$ m³ are also shown in Fig. 4. With $V_B = 0.8$ and $10 \,\mu\text{m}^3$, the system is monostable for $k_{EX} \gtrsim 0.2 \,\text{s}^{-1}$, and hence switching times are not shown in this regime. Each switching rate is obtained from 1000 independent trajectories. To see this figure in color, go online.

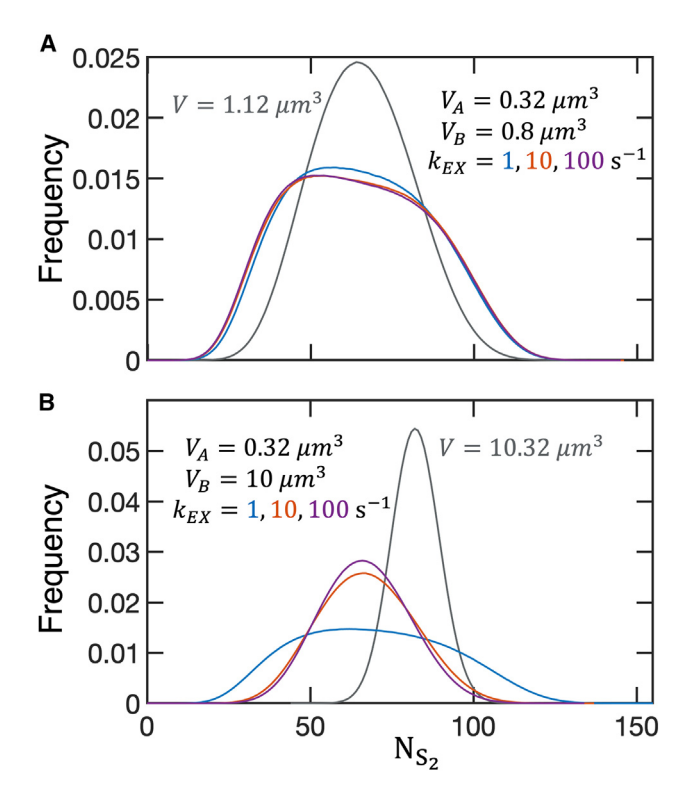


FIGURE 9 Distribution of N_{S_2} for two compartments and the equivalent single-compartment system with total volume $V=V_A+V_B$. The total number of particles is equal in each system. The two-compartment system is considered in the regime of rapid exchange, with $k_{EX}=1$, 10, and $100 \, {\rm s}^{-1}$. To facilitate comparison, the distribution for the two-compartment system corresponds to the total number of S_2 particles in both compartments. Results are shown for (A) $V_A=0.32 \, \mu {\rm m}^3$, $V_B=0.8 \, \mu {\rm m}^3$ and $(B) \, V_A=0.32 \, \mu {\rm m}^3$, $V_B=10 \, \mu {\rm m}^3$. To see this figure in color, go online.

the mean switching time depends nonmonotonically on the exchange rate of proteins between compartments. Surprisingly, the most frequent stochastic switching occurs at intermediate exchange rates, revealing a nontrivial impact of protein exchange on emergent behavior of the reaction network. More detailed analysis revealed the importance of fluctuations in the balance of kinases and phosphatases in the compartments, which impacted the nature of the steady states and the stochastic switching between them.

At low exchange rates, the states of the compartments were negatively correlated, and the mean switching time was only weakly influenced by the volume, in contrast with isolated compartments. These results are a consequence of fluctuations in enzyme numbers: when one compartment has an excess of kinases ($\Delta_{EP} > 0$), the other has an excess of phosphatases ($\Delta_{EP} < 0$). An excess of kinases promotes the active state, while an excess of phosphatases promotes the inactive state. Furthermore, increasing the exchange rate decreases the average time during which Δ_{EP} remains positive or negative, leading to an increase in the frequency of switching. At intermediate exchange rates, the mean switching time was far shorter than that of an isolated compartment. However, at larger exchange rates, the two-compartment system

behaved more like a single, well-mixed volume, leading to a marked increase in the mean switching time. In this regime, fluctuations in the balance of enzymes occur faster than the response time of the reaction network. Interestingly, when the two compartments had different effective concentrations of particles, the coupled behavior was markedly different than the behavior of a single, well-mixed volume with the same overall concentration.

These results demonstrate that compartmentalization and protein exchange can act as regulatory mechanisms for signaling networks. They also highlight the importance of fluctuations in the balance of kinases and phosphatases for phosphoregulation networks. The fluctuations impact both the steady states and the stochastic switching between them. Our study focused on compartments of similar volume containing similar numbers of proteins. However, the results suggest that even if multiple small compartments were embedded in a much larger compartment, the behavior of each small domain would be impacted by fluctuations that lead to enzyme imbalances.

Our results highlight the importance of characterizing and accounting for the exchange rate in compartmentalized systems. We found that changes in the rate can lead to qualitative changes in behavior, such as changes in the number of stable steady states. This also suggests that controlling the exchange of proteins between compartments could be an additional control mechanism used by cells or exploited in synthetic systems to expand the range of behavior of signaling networks. In cells, for example, the shuttling of MAPK proteins between the nucleus and cytoplasm can change in response to environmental conditions (25). Recent work used synthetic condensates as scaffolds to recruit signaling proteins (9), suggesting new avenues through which compartmentalization can be rationally designed to modulate the behavior of biochemical reaction networks. Computational approaches will be useful for understanding and designing responses in such systems, where the number and size of compartments, as well as the exchange of biomolecules, can potentially be controlled and dynamically modulated. It would be useful for future computational studies to investigate a variety of signaling motifs in systems with multiple compartments, which will help to reveal general principles by which compartmentalization impacts biochemical reaction networks.

SUPPORTING MATERIAL

Supporting material can be found online at https://doi.org/10.1016/j.bpj. 2024.01.039.

AUTHOR CONTRIBUTIONS

H.N.S. and S.M.A. designed the research. H.N.S., T.K.G., and E.E.L. performed the research. H.N.S., T.K.G., and S.M.A. analyzed data and wrote the manuscript.

ACKNOWLEDGMENTS

This work was supported by the National Science Foundation (PHY-1753017).

DECLARATION OF INTERESTS

The authors declare no competing interests.

REFERENCES

- Hyman, A. A., C. A. Weber, and F. Jülicher. 2014. Liquid-liquid phase separation in biology. *Annu. Rev. Cell Dev. Biol.* 30:39–58.
- Shin, Y., and C. P. Brangwynne. 2017. Liquid phase condensation in cell physiology and disease. *Science*. 357, eaaf4382.
- Takahashi, K., S. Tănase-Nicola, and P. R. Ten Wolde. 2010. Spatiotemporal correlations can drastically change the response of a MAPK pathway. *Proc. Natl. Acad. Sci. USA*. 107:2473–2478.
- Abel, S. M., J. P. Roose, ..., A. K. Chakraborty. 2012. The membrane environment can promote or suppress bistability in cell signaling networks. J. Phys. Chem. B. 116:3630–3640.
- Mugler, A., F. Tostevin, and P. R. Ten Wolde. 2013. Spatial partitioning improves the reliability of biochemical signaling. *Proc. Natl. Acad. Sci.* USA. 110:5927–5932.
- Lawley, S. D., and J. P. Keener. 2016. Including Rebinding Reactions in Well-Mixed Models of Distributive Biochemical Reactions. *Biophys. J.* 111:2317–2326.
- Tenenbaum, D., J. I. Marrone, A. C. Ventura..., 2020. Robustness in spatially driven bistability in signaling systems. Sci. Rep. 10, 5591.
- Fanger, G. R. 1999. Regulation of the MAPK family members: role of subcellular localization and architectural organization. *Histol. Histopa-thol.* 14:887–894.
- Sang, D., T. Shu, ..., L. J. Holt. 2022. Condensed-phase signaling can expand kinase specificity and respond to macromolecular crowding. *Mol. Cell.* 82:3693–3711.e10.
- Xiao, Q., C. K. McAtee, and X. Su. 2022. Phase separation in immune signalling. Nat. Rev. Immunol. 22:188–199.
- Alam-Nazki, A., and J. Krishnan. 2015. Spatial control of biochemical modification cascades and pathways. *Biophys. J.* 108:2912–2924.
- Prior, I. A., and J. F. Hancock. 2012. Ras trafficking, localization and compartmentalized signalling. Semin. Cell Dev. Biol. 23:145–153.
- O'Flynn, B. G., and T. Mittag. 2021. The role of liquid–liquid phase separation in regulating enzyme activity. *Curr. Opin. Cell Biol.* 69:70–79.
- Wang, B., L. Zhang, F. Zhou..., 2021. Liquid–liquid phase separation in human health and diseases. Signal Transduct. Targeted Ther. 6, 290.
- Klosin, A., F. Oltsch, ..., C. Zechner. 2020. Phase separation provides a mechanism to reduce noise in cells. *Science*. 367:464

 –468.
- Bauermann, J., S. Laha, ..., C. A. Weber. 2022. Chemical Kinetics and Mass Action in Coexisting Phases. J. Am. Chem. Soc. 144:19294– 19304.
- McAffee, D. B., M. K. O'Dair, ..., J. T. Groves. 2022. Discrete LAT condensates encode antigen information from single pMHC: TCR binding events. *Nat. Commun.* 13:7446.
- Shelby, S. A., I. Castello-Serrano, ..., S. L. Veatch. 2023. Membrane phase separation drives responsive assembly of receptor signaling domains. *Nat. Chem. Biol.* 19:750–758.
- Duso, L., and C. Zechner. 2020. Stochastic reaction networks in dynamic compartment populations. *Proc. Natl. Acad. Sci. USA*. 117:22674–22683.
- Norred, S. E., P. M. Caveney, ..., M. L. Simpson. 2018. Macromolecular crowding induces spatial correlations that control gene expression bursting patterns. ACS Synth. Biol. 7:1251–1258.

- Chauhan, G., S. E. Norred, ..., S. M. Abel. 2022. Crowding-Induced Spatial Organization of Gene Expression in Cell-Sized Vesicles. ACS Synth. Biol. 11:3733–3742.
- Orton, R. J., O. E. Sturm, ..., W. Kolch. 2005. Computational modelling of the receptor-tyrosine-kinase-activated MAPK pathway. *Biochem. J.* 392:249–261.
- Ferrell, J. E. 1996. Tripping the switch fantastic: how a protein kinase cascade can convert graded inputs into switch-like outputs. *Trends Biochem. Sci.* 21:460–466.
- Huang, C.-Y., and J. E. Ferrell. 1996. Ultrasensitivity in the mitogenactivated protein kinase cascade. *Proc. Natl. Acad. Sci. USA*. 93:10078–10083.
- Harrington, H. A., E. Feliu, ..., M. P. H. Stumpf. 2013. Cellular compartments cause multistability and allow cells to process more information. *Biophys. J.* 104:1824–1831.
- Courtney, A. H., W.-L. Lo, and A. Weiss. 2018. TCR Signaling: Mechanisms of Initiation and Propagation. *Trends Biochem. Sci.* 43:108–123.
- Ferrell, J. E., and R. R. Bhatt. 1997. Mechanistic studies of the dual phosphorylation of mitogen-activated protein kinase. *J. Biol. Chem.* 272:19008–19016.
- Ortega, F., J. L. Garcés, ..., M. Cascante. 2006. Bistability from double phosphorylation in signal transduction: kinetic and structural requirements. FEBS J. 273:3915–3926.
- Feng, S., M. Sáez, ..., O. S. Soyer. 2016. Core signalling motif displaying multistability through multi-state enzymes. J. R. Soc. Interface. 13, 20160524
- Arkun, Y., and M. Yasemi. 2018. Dynamics and control of the ERK signaling pathway: Sensitivity, bistability, and oscillations. *PLoS One.* 13, e0195513.
- Markevich, N. I., J. B. Hoek, and B. N. Kholodenko. 2004. Signaling switches and bistability arising from multisite phosphorylation in protein kinase cascades. *J. Cell Biol.* 164:353–359.
- 32. Chatterjee, A., Y. N. Kaznessis, and W.-S. Hu. 2008. Tweaking biological switches through a better understanding of bistability behavior. *Curr. Opin. Biotechnol.* 19:475–481.
- 33. van Kampen, N. 2007. Stochastic Processes in Physics and Chemistry. Elsevier, Amsterdam.
- 34. Endres, R. G. 2015. Bistability: requirements on cell-volume, protein diffusion, and thermodynamics. *PLoS One.* 10, e0121681.
- Goldbeter, A. 2018. Dissipative structures in biological systems: bistability, oscillations, spatial patterns and waves. *Philos. Trans. A Math. Phys. Eng. Sci.* 376, 20170376.
- Donovan, R. M., A. J. Sedgewick, ..., D. M. Zuckerman. 2013. Efficient stochastic simulation of chemical kinetics networks using a weighted ensemble of trajectories. J. Chem. Phys. 139, 115105.
- Tse, M. J., B. K. Chu, E. L. Read..., 2018. Rare-event sampling of epigenetic landscapes and phenotype transitions. *PLoS Comput. Biol.* 14, e1006336.
- Das, J., M. Kardar, and A. K. Chakraborty. 2009. Positive feedback regulation results in spatial clustering and fast spreading of active signaling molecules on a cell membrane. J. Chem. Phys. 130, 245102.
- Mlynarczyk, P. J., R. H. Pullen, III, and S. M. Abel. 2016. Confinement and diffusion modulate bistability and stochastic switching in a reaction network with positive feedback. *J. Chem. Phys.* 144, 015102.
- Gillespie, D. T. 2007. Stochastic simulation of chemical kinetics. *Annu. Rev. Phys. Chem.* 58:35–55.
- Gunawardena, J. 2005. Multisite protein phosphorylation makes a good threshold but can be a poor switch. *Proc. Natl. Acad. Sci. USA*. 102:14617–14622.
- Harrington, H. A., M. Komorowski, ..., M. P. H. Stumpf. 2012. Mathematical modeling reveals the functional implications of the different nuclear shuttling rates of Erk1 and Erk2. *Phys. Biol.* 9, 036001.

- 43. Zhang, Y., A. G. Pyo, N. S. Wingreen..., 2023. Interface resistance of biomolecular condensates. Elife. 12, RP91680.
- 44. Hubatsch, L., L. M. Jawerth, ..., C. A. Weber. 2021. Quantitative theory for the diffusive dynamics of liquid condensates. Elife. 10, e68620.
- 45. Levine, J., H. Y. Kueh, and L. Mirny. 2007. Intrinsic fluctuations, robustness, and tunability in signaling cycles. Biophys. J. 92:4473-4481.
- 46. Metzner, P., C. Schütte, and E. Vanden-Eijnden. 2009. Transition Path Theory for Markov Jump Processes. Multiscale Model. Simul. 7:1192–1219.
- 47. Su, X., J. A. Ditlev, ..., R. D. Vale. 2016. Phase separation of signaling molecules promotes T cell receptor signal transduction. Science. 352:595-599.
- 48. Crowe, C. D., and C. D. Keating. 2018. Liquid-liquid phase separation in artificial cells. Interface Focus. 8, 20180032.